Nanoscale

PAPER

View Article Online
View Journal

Cite this: DOI: 10.1039/d6nr00361c

In-plane mechanical properties of terephthalate-based two-dimensional metal–organic frameworks

Shengjia Zhang, †[a] Kamal E. S. Nassar, †[b] Ali Azmy, [b] Lukasz Wojtas,[b] Ioannis Spanopoulos *[b] and Qing Tu *[a]

Two-dimensional (2D) metal–organic frameworks (MOFs) are often subjected to mechanical loading in their applications, and the in-plane elastic modulus $E_{\parallel}$ is a critical material property needed to understand and predict the mechanical behaviors of 2D MOFs for improved mechanical reliability and strain engineering of their functional properties. However, the $E_{\parallel}$ values of 2D MOFs are largely unknown, even for those with widely used coordination linkers like 1,4-benzenedicarboxylate (BDC), because of the challenges in in-plane mechanical testing imposed by both the extreme dimensionality and the high sensitivity of 2D MOFs to external factors (*e.g.*, e-beams) due to their hybrid organic–inorganic nature. Here we employed atomic force microscopy (AFM) stretching of suspended thin membranes to measure the $E_{\parallel}$ of three structurally related, BDC-coordinated MOFs. The 2D $Zn_3(BDC)_3(H_2O)_2{\cdot}4(DMF)$ (DMF = *N*,*N*-dimethylformamide) has an $E_{\parallel}$ value of 11.2 ± 2.5 GPa, much lower than that of its 3D analog, $(DMA)_2[Zn_3(BDC)_4{\cdot}1.5H_2O]$ (DMA = dimethylammonium) ($E_{\parallel}$ = 25.9 ± 6.3 GPa), owing to the absence of interlayer covalent bonding. However, a 2D Mn analog, $Mn_3(BDC)_3{\cdot}4(DMF)$, exhibits enhanced in-plane stiffness ($E_{\parallel}$ = 25.5 ± 4.9 GPa), likely originating from the strengthened coordination at the nodes. We further compared 2D MOFs to other 2D materials and widely used engineering material systems using a density *vs.* $E_{\parallel}$ Ashby plot. Our results provide indispensable insights into the structure–mechanical property relationship of 2D MOFs to guide material engineering and selection.

Received 27th January 2026,
Accepted 13th April 2026

DOI: 10.1039/d6nr00361c

rsc.li/nanoscale

Introduction

Metal–organic frameworks (MOFs) are a family of porous crystalline materials that combine metal ions with coordinated organic ligands to form complex structures enabling huge potential in a wide range of applications, including gas storage, catalysis, and chemical separations.[1–4] The tremendous chemical space available to these materials, together with the solution processability, allows for facile design of MOF structures with tailored functionality.[5] The success of two-dimensional (2D) materials further inspired the engineering of MOFs into 2D layered compounds to relax the structural constraints and expand the functional properties and architectural design space.[6–8] Integration of MOFs and other low-dimensional materials into novel heterostructures *via* clean van der Waals (vdW) interfaces is thus possible and has resulted in new promising applications.[6,9] Hence, interlayer interfaces become a new playground for tuning material properties (*e.g.*, intercalation and sliding).[6]

In all these applications, 2D MOFs are often subjected to mechanical loading during device fabrication and operation,[10–12] such as compression, dilation, stretching, bending, twisting, *etc.*, where the elastic modulus E is a critical mechanical property needed to understand and predict the mechanical behaviors of 2D MOFs in order to mitigate mechanical failure and improve the mechanical reliability of MOF-based applications. Moreover, mechanical strain can also be harnessed to enhance the functional performance of 2D MOFs or to tailor the properties of the materials interfacing with 2D MOFs.[6,13,14] Knowing the E of 2D MOFs is the first step to achieve precisely controlled strain engineering. The abundant chemistry involving hybrid organic–inorganic bonds, which differ from those in conventional materials such as metals, ceramics, and polymers,[10,15] further calls for the exploration of the structure–property relationships of 2D MOFs regarding their mechanical behavior.

Because of both the fundamental importance and practical need, significant efforts have been devoted to studying the

[a]*Department of Material Science and Engineering, Texas A&M University, College Station, TX 77840, USA. E-mail: qing.tu@tamu.edu*
[b]*Department of Chemistry, University of South Florida, Tampa, FL, 33620, USA. E-mail: spanopoulos@usf.edu*
† These authors contributed equally.

mechanical properties of 3D MOFs,[10,11] mainly utilizing small-scale mechanical techniques like instrumented nanoindentation and atomic force microscopy (AFM) due to the small sample size; however, the mechanical study still significantly lags behind other functional property studies of these materials. Such small-scale techniques are applicable to study the out-of-plane (*i.e.*, perpendicular to the basal planes of the molecular sheets) mechanical properties of 2D MOFs, owing to the layered structure. However, evaluating the in-plane mechanical properties is more challenging. First, directly applying nanoindentation or AFM-based indentation techniques along the in-plane directions violates the assumptions of analysis methods due to the in-plane *vs.* out-of-plane mechanical anisotropy of these materials.[16,17] Although many studies still employed these indentation techniques neglecting this fact to probe the in-plane directions,[12,18–20] the reported results are questionable. Second, the small sample size and high susceptibility to damage from other factors present during the measurements (*e.g.*, electron beam or humidity) render many in-plane testing techniques widely used in 2D materials not feasible for 2D MOFs. Because of these challenges, only a handful of reliable reports about the in-plane mechanical properties of 2D MOFs are available in the literature to date,[21–26] despite the fact that in-plane is the main loading direction for 2D MOFs in practical applications owing to the layered structure. While 2D MOFs and their corresponding 3D counterparts can share the same metal–organic bonds and connectivity in-plane,[6] where the metal–organic-ligand architecture, rather than the weak van der Waals (vdW) interface (as in the out-of-plane direction), is still the main load carrier, it remains unclear how the transition of the structure from 3D to 2D will affect the in-plane elastic modulus $E_{\parallel}$. This is largely due to the lack of a direct comparison of the in-plane elastic moduli of 2D and 3D MOFs. This knowledge gap hinders our ability to leverage the abundant structure–mechanical property studies of 3D MOFs[10–12] for designing 2D analogs. Furthermore, although it is common to substitute the metal ions in the MOF structure while maintaining the coordination ligands and topology,[6] the influence of such modification on the $E_{\parallel}$ of 2D MOFs is still elusive.

Here, we measure the $E_{\parallel}$ of 2D MOFs coordinated by the 1,4-benzenedicarboxylate (BDC) linker. This is one of the most widely used organic linkers in MOF chemistry.[27] Its rigid and linear geometry supports predictable coordination environments and reproducible framework topologies,[28] which have enabled the development of numerous benchmark MOF systems such as MOF-5[29] and UiO-66.[30] Therefore, BDC-based frameworks provide a structurally reliable and broadly representative platform for probing the intrinsic mechanical behavior of layered MOFs and establishing insights that are transferable to other 2D coordination polymer systems.[28] However, to date, the mechanical properties of 2D MOFs based on BDC linkers have not been investigated.[11]

We use AFM stretching of suspended thin 2D MOF membranes to measure their $E_{\parallel}$. This method has been used to reliably quantify the $E_{\parallel}$ of various 2D materials,[31–34] including 2D materials with hybrid bonds[35,36] or coordination polymers[37] similar to 2D MOFs. We first compare the $E_{\parallel}$ of the 2D MOF $Zn_3(BDC)_3(H_2O)_2{\cdot}4(DMF)$ (DMF = *N*,*N*-dimethylformamide) with that of its 3D analog, $(DMA)_2[Zn_3(BDC)_4{\cdot}1.5H_2O]$ (DMA = dimethylammonium), to uncover the impact of structural transition from 3D to 2D on the elastic property. Furthermore, we replace Zn with Mn in the 2D MOF while maintaining the same framework connectivity to examine the effects of metal ions on the elastic modulus. These measurements, together with the comparison with other relevant layered materials and classical materials widely adopted in engineering applications, provide indispensable insights into the in-plane structure–mechanical property relationship of 2D MOFs and materials selection for applications.

Experimental section

Materials synthesis

All MOF materials were synthesized by solution-based methods and characterized by single crystal and powder X-ray diffraction (XRD) to confirm the success of synthesis (Fig. 1 and 2, and Supplementary Information (SI) – Section 1). Briefly, for the 3D MOF, $(DMA)_2[Zn_3(BDC)_4{\cdot}1.5H_2O]$ (abbreviated as 3D-Zn-MOF below), 0.07 mmol of terephthalic acid were dissolved in 3 mL of DMF and 1 mL of ethanol in a 20 mL glass vial under heating (150 °C hot plate temperature). Then, 0.07 mmol of $Zn(NO_3)_2{\cdot}6H_2O$ and three drops of concentrated nitric acid were added. The heating decomposed DMF into DMA, which served as counter cations to stabilize and charge balance the structure. The solution was then kept at 85 °C overnight in an isothermal oven, yielding colorless crystals upon cooling to room temperature. This growth method was then slightly modified to produce the 2D MOF, $Zn_3(BDC)_3(H_2O)_2{\cdot}4(DMF)$ (abbreviated as 2D-Zn-MOF below). In this case, 0.07 mmol of terephthalic acid was dissolved in 6 mL of DMF and 1 mL of ethanol under sonication. After adding one drop of nitric acid and 0.07 mmol of Zn $(NO_3)_2{\cdot}6H_2O$, the mixture was heated at 85 °C in an isothermal oven overnight to yield transparent crystals. The synthesis of 2D $Mn_3(BDC)_3{\cdot}4(DMF)$ (abbreviated as 2D-Mn-MOF below) followed a published protocol.[38]

AFM stretching of suspended MOF membranes

AFM experiments were conducted following our reported protocol.[35,39] Briefly, thin MOF membranes were mechanically exfoliated *via* scotch tape[40] and transferred to freshly cleaned SiO_2/Si wafer with patterned holes inside a N_2-filled glovebox. The exfoliation is very straightforward for 2D MOFs owing to the weak interlayer interfaces in the crystals (Fig. 1C). We found that the 3D-Zn-MOF can also be exfoliated by this method, producing thin membranes with crystal orientations similar to those of the 2D-Zn-MOF, probably because the interlayer bonds are not that strong and the density of the bonds is not high (see Fig. 1F). However, such interlayer bonds are still much stronger than the vdW interactions in the 2D-Zn-MOF,

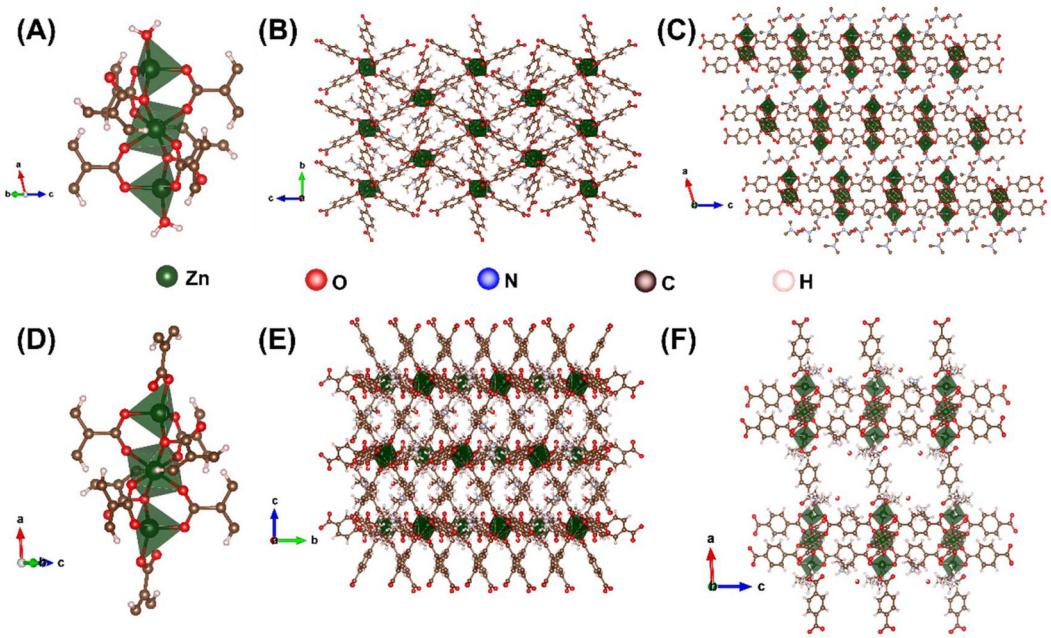

Fig. 1 Crystal structure of the Zn MOFs tested in this study: Top: 2D $Zn_3(BDC)_3(H_2O)_2{\cdot}4(DMF)$. (A) The inorganic part of the material and projection of the crystal structure along the (B) *a*-axis and (C) *b*-axis. Bottom: 3D $(DMA)_2[Zn_3(BDC)_4{\cdot}1.5H_2O]$. (D) The inorganic part of the material and projection of the crystal structure along the (E) *a*-axis and (F) *b*-axis.

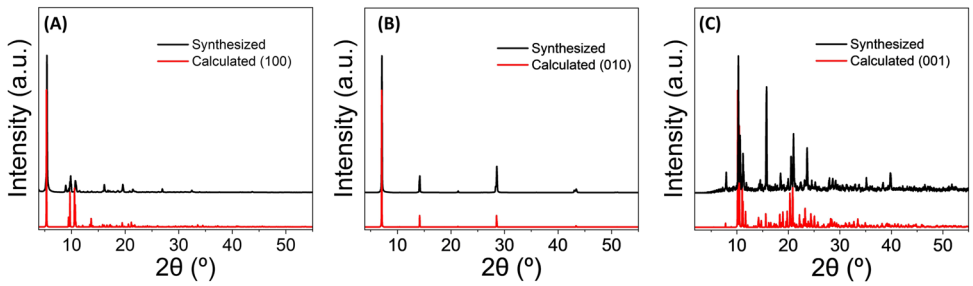

Fig. 2 PXRD spectra of the tested MOFs: (A) 3D-Zn-MOF, (B) 2D-Zn-MOF, and (C) 2D-Mn-MOF. The red spectra are calculated from the solved single-crystal structures of the MOFs.

which results in a much lower yielding rate of successful transfer of the 3D-Zn-MOF than the 2D version.

All AFM measurements were performed using an Asylum MFP-3D Infinity AFM (Asylum Research, Oxford Instruments, CA) with AC240TS (Olympus) probes under dry air flow. Before the AFM measurements, the deflection sensitivity of the AFM cantilever was calibrated by recording the indentation force curve of the cantilever on a clean silicon surface. The spring constant k_c of the AFM cantilever was then calibrated by fitting the first free resonance peak of the cantilever to the simple harmonic oscillator equation[41] to measure the power spectral density of the thermal noise fluctuations in air.[42] The indentation rate was kept at 100 nm s^{-1} to avoid high-rate-induced noise.[35] The membranes with hysteresis or sliding features in the loading and unloading curves were excluded. At least 10 membranes from two distinct crystals were measured for each type of MOF tested here.

Results and discussion

Targeting the synthesis of 2D MOFs, we selected Zn-based analogs on BDC ligands, which are extensively explored. The 2D-Zn-MOF and the 2D-Mn-MOF have been reported in the literature before,[38,43] as well as the framework of the 3D-Zn-MOF.[44] However, the reported structure of the latter does not have the correct formula necessary for a charge balanced structure. Hence, in this work, we synthesized and characterized the material by XRD to identify the correct structure and formula, given their importance for understanding underlying structure–property relationships, especially given the ultra-fine nature of the targeted mechanical properties. Note that, in this work, we use the 2D and 3D notations to refer to the degree of coordination of the MOF.[45] In a 2D MOF, coordination bonds will span across two directions forming layers, which would not be connected through coordination bonds, rather through

weak interactions. In a 3D MOF, coordination bonds extend in all three spatial directions. Therefore, the use of the terms 2D and 3D MOFs does not refer to exfoliated single-layer frameworks. The flakes used in the mechanical studies contain multiple layers of the corresponding 2D and 3D MOFs (see below in the mechanical test part), and not a single constituent layer of the materials.

By adjusting the reaction conditions, we managed to synthesize 2D and 3D Zn-based frameworks. Starting with the structure of the 2D-Zn-MOF, it was determined by single-crystal X-ray diffraction (SC-XRD) studies that the material crystalized in the centrosymmetric space group $P2_1/c$. The secondary building unit of the structure features a trinuclear metal cluster consisting of three Zn^{2+} cations, four terephthalate (BDC) ligands and two water molecules. The Zn^{2+} cations are vertically aligned across the layer and connected through the carboxylate groups of BDC. The central Zn^{2+} cation is in centrosymmetric octahedral coordination with six oxygen atoms derived from six different carboxylate groups, whereas the two terminal Zn^{2+} cations have a coordination number of 4 instead of 6 where three oxygen atoms derived from three carboxylate groups are coordinated to the Zn^{2+} cation and the metal node is terminated with one water molecule (Fig. 1A). The structure is completed with two DMF solvent molecules that are hydrogen bonded to each of the terminal water molecules of the metal nodes at a distance of 1.75 Å, giving rise to the layered 2D framework with an overall formula of $Zn_3(BDC)_3(H_2O)_2{\cdot}4(DMF)$ as shown in Fig. 1B and C. By examining the bonding scheme of the metal clusters, it was found that the Zn–O bond length ranges from 2.035 Å to 2.204 Å for the central octahedron, whereas Zn–O bond lengths in the terminal tetrahedra were found to be 1.940 Å, 1.944 Å, 1.967 Å, and 2.009 Å. While the distance between adjacent Zn^{2+} cations within the same trinuclear metal cluster is 3.249 Å, Zn metal clusters lie at a distance of 10.41 Å measured between the central Zn cations of the clusters. Moreover, the 2D layers are stacked along the *c*-axis, with a distance of 4.62 Å between the terminating water molecules of the metal cluster, while DMF molecules lie between the layers and connect them through hydrogen bonding.

Shifting the focus to the 3D structure, it was found from SC-XRD that the material crystallized in the monoclinic $C2/c$ space group having a twofold rotation axis perpendicular to two glide planes. The structure features the same metal cluster as the 2D material discussed above with the exception of replacing the two terminal water molecules with one monodentate BDC ligand bridging between the layers forming a 3D framework (Fig. 1E and F). Consequently, the metal cluster of this structure consists of three Zn^{2+} cations with two different coordination modes similar to the 2D structure. The central cation is coordinated to six oxygen atoms of six different BDC molecules that are shared with other Zn^{2+} cations forming an octahedron, whereas the two terminal metal cations are coordinated to four oxygens derived from four BDC molecules forming tetrahedra and connecting the metal nodes across the three dimensions. Two disordered protonated DMA molecules lie inside the cavity forming a 3D framework with the overall formula $(DMA)_2[Zn_3(BDC)_4{\cdot}1.5H_2O]$ (Fig. 1D). In terms of the bonding scheme, Zn–O bond lengths for the central and terminal clusters are almost identical to those of the 2D structure. Specifically, the Zn–O bond length of the central octahedron ranges from 2.037 Å to 2.244 Å while the bond lengths of the two terminal tetrahedra are 1.947 Å, 1.965 Å, 1.976 Å, and 1.985 Å. Furthermore, the interatomic distances between the metal centers are also similar to those of the 2D structure, where the distance between the central and terminal Zn^{2+}

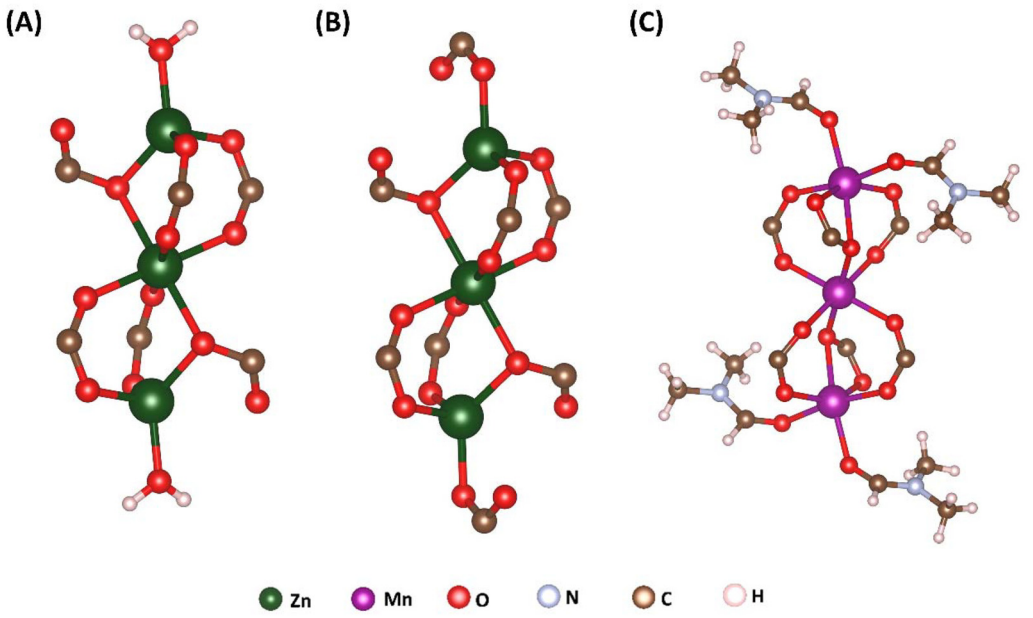

Fig. 3 Metal node coordination environment for (A) 2D-Zn-MOF, (B) 3D-Zn-MOF, and (C) 2D-Mn-MOF.

cations is 3.266 Å, and the distance between the closest terminal metal cations of two different metal clusters is 10.36 Å.

Notably, the 2D-Zn-MOF and 2D-Mn-MOF share an almost identical structure[38] (Fig. 1C and S1B), except that the 2D-Zn-MOF contains some H_2O molecules in the cavities while the 2D-Mn-MOF does not (see the chemical formula in the synthesis part). Powder XRD (PXRD) measurements were used to confirm phase purity (Fig. 2), revealing that the calculated and experimental PXRD patterns are identical.

Fig. 3 illustrates the distinct coordination environments of the three MOFs investigated here: 2D-Zn-MOF, 3D-Zn-MOF, and 2D-Mn-MOF. The two Zn-based MOFs share structural similarities but differ primarily in their terminal ligands. In the 2D-Zn-MOF, aqua ligands (H_2O) serve as terminal linkers, while the Zn^{2+} centers in the 3D-Zn-MOF coordinate exclusively with BDC linkers, which bridge adjacent layers covalently (Fig. 3A and B). Consequently, the layers of 2D-Zn-MOF, although terminated by aqua ligands, are held together by vdW interactions, yielding a two-dimensional architecture with weak interlayer interactions. In contrast, the layers of 3D-Zn-MOF are covalently interconnected through BDC linkers, giving rise to a fully three-dimensional framework (Fig. 3B). The 2D-Mn-MOF presents a markedly different structural motif at the coordination nodes. It is built around a trinuclear metal cluster in which all three Mn^{2+} centers are six-coordinate, yet with differentiated ligand environments. The central Mn^{2+} octahedron is coordinated exclusively by six BDC linkers, whereas each of the two terminal Mn^{2+} octahedra coordinate with three BDC linkers and two DMF molecules, with the latter acting as terminal ligands that enforce layer separation and stabilization through vdW interactions (Fig. 3C).

Thin flakes of MOFs transferred to the patterned silicon wafer were first identified using an optical microscope (*e.g.*, Fig. 4B, S2A and S2E). The flakes were then imaged by tapping mode AFM (Fig. 4C, S2B and S2F) to measure the thickness of the membrane and precisely position the AFM tip to the center of the membrane for a nanomechanical test, as illustrated in Fig. 4A. Membranes with a thickness between 10 and 30 nm (Fig. 4C (inset), S2D and S2H) were selected for the test because: (1) the flake is sufficiently thick to ensure that any

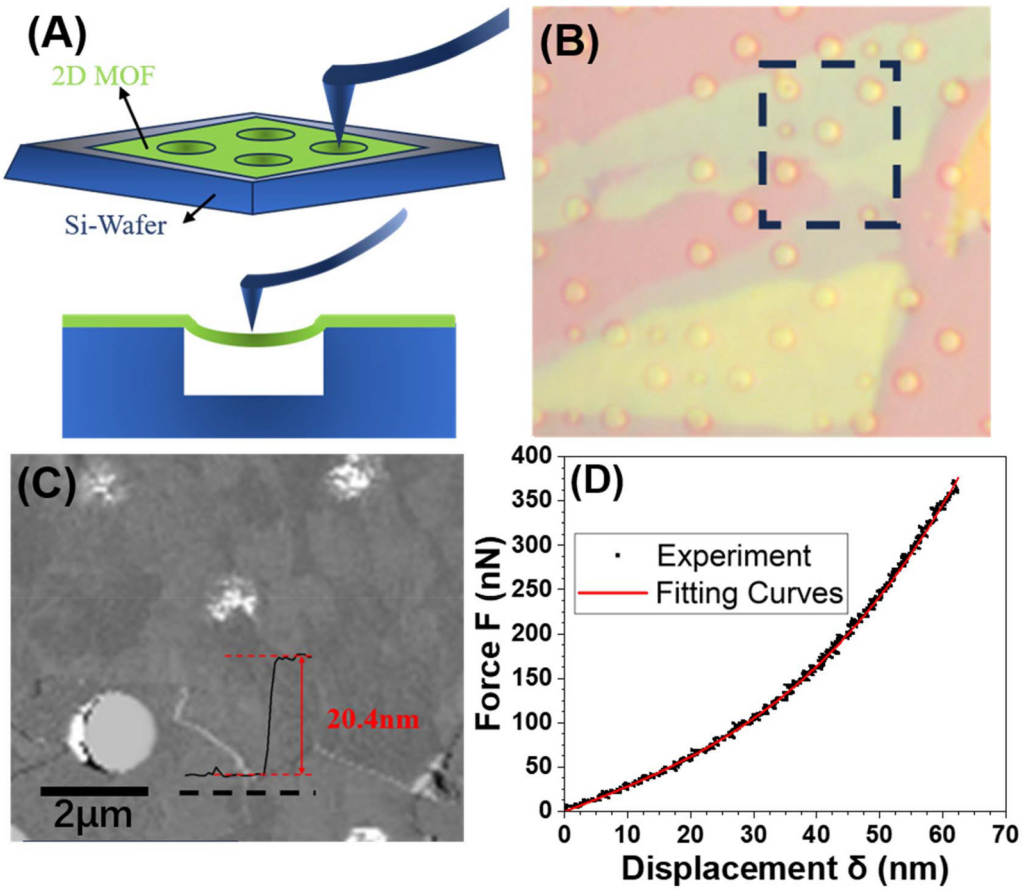

Fig. 4 Measuring the $E_{\|}$ of suspended MOF membranes by AFM: (A) schematic illustrating AFM stretching of suspended thin MOF membranes to extract $E_{\|}$. (B) Representative optical image showing thin MOF membranes (2D-Mn-MOF here) transferred on the hole-patterned silicon wafer. (C) The tapping mode AFM amplitude image of the region marked with the dashed box in (B). The amplitude image gives better visualization of the suspended region. The inset is the height profile along the dashed line in (C), showing the thickness of the flake. (D) The experimentally obtained F–δ curve fitted using eqn (2).

softening effects due to potential interlayer sliding will be saturated and the measured $E_{\parallel}$ values represent the values of the bulk crystals,[32,35,46] as further confirmed by no clear thickness dependence of $E_{\parallel}$ in the tested range (Fig. S3); and (2) the flake is thin enough such that the widely used analysis model is still applicable.[31,35,47] As the AFM tip stretched the center of the membrane in the Z direction, the applied force F and the total moving distance of the piezo in the vertical direction Z_{piezo} were collected. The membrane's actual deformation δ is then determined as:

$$\delta = Z_{\text{piezo}} - \delta_{\text{tip}} \tag{1}$$

where $\delta_{\text{tip}} = F/k_c$ represents the deflection of the AFM tip.

Under such loading conditions, the deformation of the suspended MOF membrane can be modeled as an isotropic continuous circular membrane with fixed edges and a point load in the center,[34,48] whose F–δ curve is described using eqn (2) below:[34,39,46]

$$F - F_0 = \left[\frac{4\pi E_{\parallel} t^3}{3(1-\nu^2)a^2}\right](\delta - \delta_0) + \sigma_0^{2D}\pi(\delta - \delta_0) + \frac{q^3 E_{\parallel} t}{a^2}(\delta - \delta_0)^3, \tag{2}$$

where t and a are the thickness and radius of the membrane, respectively; σ_0^{2D} represents the pre-tension in the membrane due to transfer; F_0 and δ_0 indicate the actual contact point when the AFM tip starts to stretch the membrane; and $q = 1/(1.05 - 0.15\nu - 0.16\nu^2)$ with ν being the Poisson's ratio of the material. Here, we take $\nu = 0.3$, which is commonly accepted for hybrid organic–inorganic framework materials like MOFs and hybrid organic–inorganic perovskites (HOIPs).[10,35,49] The first term represents the bending of the membrane while the 2nd term is the mechanical response of a membrane with pre-tension. The last term arises from the in-plane stretching of the membrane. The experimentally obtained F–δ data are fitted to eqn (2) with $E_{\parallel}$, F_0, σ_0^{2D} and δ_0 taken as fitting parameters to extract $E_{\parallel}$ values. Representative data (Fig. 4D, S2C and S2G) demonstrate excellent agreement between the experimental results and the model, confirming the appropriateness of the model used here.

Fig. 5A–C show the histograms of the measured $E_{\parallel}$ for each MOF tested, which generally follows a Gaussian distribution. Fig. 5D shows the mean values and standard deviation of the data. The $E_{\parallel}$ value of the 3D-Zn-MOF is 25.9 ± 6.3 GPa, which falls in the range of reported E values of 3D MOFs.[10,12] In comparison, the 2D-Zn-MOF exhibits a much lower $E_{\parallel}$ (11.2 ± 2.5 GPa). Although the 3D-Zn-MOF has a slightly lower amount

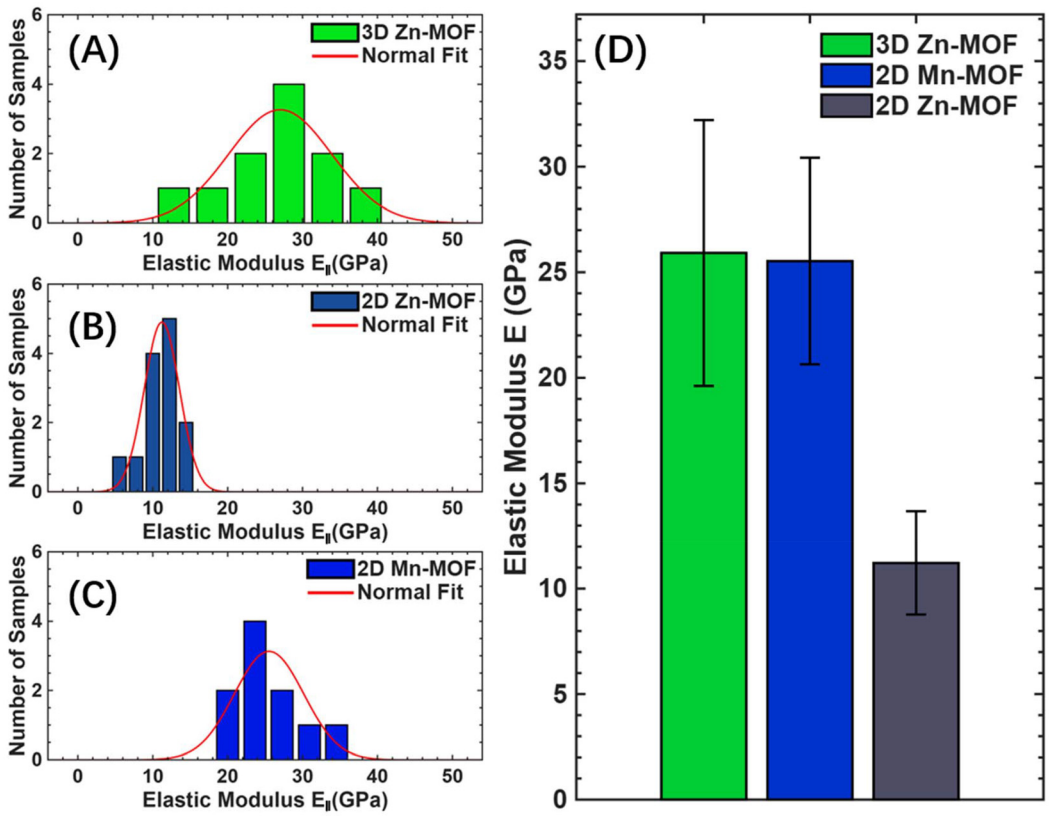

Fig. 5 Measured in-plane elastic moduli of MOFs tested here: (A), (B) and (C) are histograms of the measured elastic modulus data points for 3D-Zn-MOF, 2D-Zn-MOF, and 2D-Mn-MOF, respectively. The histograms are fitted with normal distributions. (D) Mean values and standard deviation of the elastic modulus data measured for each MOF tested here.

of H_2O in the structure, more small molecules filling the porous structure in MOFs typically gives higher stiffness.[50] The observed significant reduction in $E_{\parallel}$ is thus unlikely due to the variation in H_2O, but rather arises from the loss of continuous load-bearing connectivity because of the elimination of covalent bonding between the layers (Fig. 1C and F), as found in HOIPs,[15] a similar family of materials. In the 3D-Zn-MOF, terephthalate linkers integrate adjacent MOF layers into an extended, crosslinked network that efficiently suppresses interlayer slip and distortion of the porous structure. This topological continuity enhances long-range stress transfer, leading to a high effective in-plane stiffness. Upon dimensional reduction to a 2D layered configuration, the absence of vertical bridging linkers can have two softening effects. First, it relaxes some deformation restrictions of the in-plane MOF structure. This relaxation can introduce additional rotational degrees of freedom at the coordination nodes, activating architectural "soft modes" that allow the porous framework to be further deformed, similar to the softening effects arising from distortion of the octahedra and the puckered structure in 2D HOIPs[46] and black phosphorus,[51] respectively. Second, eliminating the interlayer linkers permits sliding between adjacent layers upon mechanical loading, which can also reduce the in-plane stiffness, as suggested by prior studies on 2D materials.[32,33,35] This further implies that tuning the interlayer interactions, *e.g.*, by engineering the molecular chemistry and structure of the organic ligands,[46] *via* intercalation chemistry,[52] or through environmental factors like temperature[39,53] that affect the interacting forces, can effectively tune the $E_{\parallel}$ of 2D MOFs, as suggested by our recent studies of 2D HOIPs.[39,46,49]

The metal ions are essential components of the coordination nodes in MOF structures and have been widely used to tailor the functional properties of MOFs while maintaining a similar porous structure.[6] Surprisingly, although the unconnected 2D layered structure is retained (Fig. S1), replacing Zn with Mn greatly increases $E_{\parallel}$ to 25.5 ± 4.9 GPa, which is almost as stiff as the 3D-Zn-MOF. This is unlikely due to the absence of H_2O in the 2D-Mn-MOF because inclusion of small molecules into the porous structure should increase $E_{\parallel}$,[50] which contradicts our observation. Similarly, the observed trend is probably not because of the interfaces since the interlayer interaction strength should be comparable owing to the same interfacial chemistry consisting of BDC ligands.

We attributed the change in $E_{\parallel}$ to the deformability of the framework architecture arising from the node coordination difference. Distortion of architectural features plays a crucial role in dictating the elastic modulus of 2D materials, as observed in black phosphorus and 2D HOIPs. The distortion

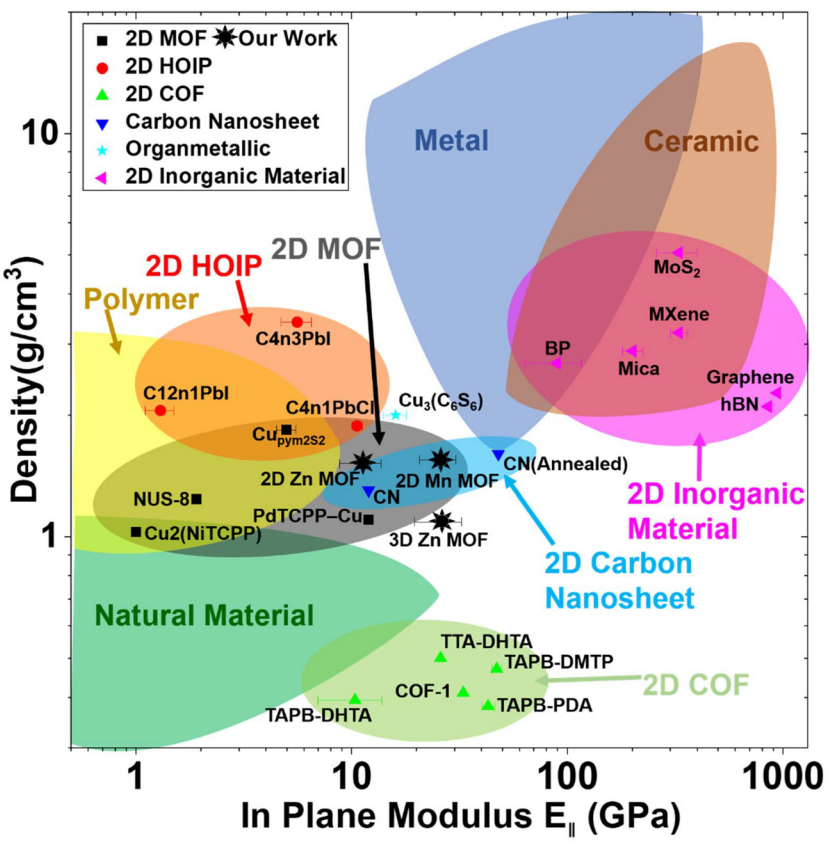

Fig. 6 Ashby plot of density *vs.* $E_{\parallel}$ with tested MOFs, other related 2D materials and main materials used in engineering applications. The ranges for natural materials, polymers, metals and ceramics are adapted from ref. 57. The ranges for 2D HOIPs are estimated based on ref. 35, 39 and 46. The material data points marked here and the corresponding references are summarized in Table S10.

of the porous MOF structure should be significantly affected by the nodes. In the tested MOF here, the nodes are formed by metal atoms coordinated to the oxygen atoms in the BDC ligands. In the 2D-Mn-MOF, the node is formed by three joint Mn–O octahedra (Fig. 3C and S1A), while in the 2D-Zn-MOF, it constitutes one Zn–O octahedron connected with two Zn–O tetrahedra (Fig. 1A and 3A). Moreover, there also differences among the coordination of BDC ligands to the terminal metal ions (monodentate *vs.* bidentate). These differences make the framework in 2D-Zn-MOF weaker and more deformable, and hence results in the structural softness. Tuning the fine features of the connection topology near the coordination nodes can be another effective route to engineer the $E_{\parallel}$ of 2D MOFs.

We put the tested materials in this study into a density *vs.* $E_{\parallel}$ Ashby plot, together with other relevant 2D materials and material categories commonly used in engineering applications (Fig. 6). Density and Young's modulus are two widely considered properties when selecting materials for applications. Owing to the molecular pores in their structure, MOFs are famous for their relatively low density compared to other condensed solids. The results from our study and earlier 2D MOFs measured through appropriate methods allow us to estimate the boundaries for 2D MOFs on this plot. As shown in Fig. 6, 2D MOFs reside closer to polymers, natural materials (*e.g.*, wood) and other hybrid materials (*e.g.*, HOIPs), featuring a much lower density and E than metals and ceramics, as a result of the inclusion of organic components and porous structures. The hybrid bonding nature and the structural softness mentioned earlier separate 2D MOFs from conventional 2D materials, which have strong, pure inorganic bonds in-plane and no/little architectural flexibility under mechanical loading. Because of the similar hybrid bonding nature and structural softness (enabled by distortion of the metal–halide octahedra in HOIPs[46]), the $E_{\parallel}$ values of 2D HOIPs and 2D MOFs are roughly in the same range, similar to their out-of-plane moduli.[15,54] However, the absence of a porous structure in 2D HOIPs gives them a slightly higher density than 2D MOFs. In comparison, the other 2D family of coordinated polymers, *i.e.*, covalent–organic frameworks (COFs),[37,55,56] are much stiffer, due to the strong covalent bonds that constitute the framework and lack of structural distortion at the nodes owing to the lack of more deformable metal-coordination structures. The absence of heavy metal elements in COFs further reduces their density compared to 2D MOFs. However, the metal elements endow 2D MOFs with many functional properties,[6] which will be challenging to engineer into COFs. Generally speaking, 2D MOFs provide material options covering the blank area in the material design space (Fig. 6) that balances softness (flexibility), functionality, and light weight to meet application needs.

Conclusions

In conclusion, we employed AFM stretching of suspended thin MOF membranes and measured the $E_{\parallel}$ of three structurally related, BDC-coordinated MOFs. The 3D-Zn-MOF exhibits an $E_{\parallel}$ value of 25.9 ± 6.3 GPa, which drops to 11.2 ± 2.5 GPa in the 2D-Zn-MOF. We attributed the in-plane stiffness reduction to the absence of interlayer covalent bonding, which not only relaxes the in-plane deformation constraints of the MOF but also allows sliding at the interlayer interfaces. In contrast, the 2D-Mn-MOF, coordinated by the same BDC linker in a similar topology to the 2D-Zn-MOF, shows a higher $E_{\parallel}$ value (25.5 ± 4.9 GPa). A careful examination of the crystal structure suggests that the enhanced stiffness in the 2D-Mn-MOF compared to the 2D-Zn-MOF is likely due to the coordination differences at the node that affect the deformability of the framework architecture. We further constructed an Ashby plot of density *vs.* E summarizing the major categories of 2D materials and other widely used engineering material systems to guide a general material selection. 2D MOFs offer material options that fill the blank area in the material design space, balancing softness, functionality, and light weight. Our results unveil the critical roles of interlayer interactions and structural deformability in dictating the in-plane stiffness of 2D MOFs, through which the mechanical behavior of 2D MOFs can be tailored leveraging the abundant chemical options available to these materials.

Conflicts of interest

There are no conflicts to declare.

Data availability

The data supporting this article have been included as part of the supplementary information (SI)

Supplementary information: details of materials synthesis and X-ray diffraction of the materials investigated, additional AFM images and representative F *vs.* δ curves, and a summary table of density *vs.* elastic moduli data used to construct the Ashby plot. See DOI: https://doi.org/10.1039/d6nr00361c.

CCDC 2522895 and 2522896 contain the supplementary crystallographic data for this paper.[58a,b]

Acknowledgements

This research was primarily supported by the National Science Foundation under Award No. CMMI-2311573 and partially supported by TAMU Division of Research – Targeted Proposal Teams - Grants on the Edge funds (S. Z. and Q. T.). I. S. acknowledges support from USF start-up funds.

References

1 J. Lee, O. K. Farha, J. Roberts, K. A. Scheidt, S. T. Nguyen and J. T. Hupp, Metal–organic framework materials as catalysts, *Chem. Soc. Rev.*, 2009, **38**(5), 1450–1459.

2 B. Li, H.-M. Wen, W. Zhou and B. Chen, Porous Metal–Organic Frameworks for Gas Storage and Separation: What, How, and Why?, *J. Phys. Chem. Lett.*, 2014, **5**(20), 3468–3479.
3 S. Qiu, M. Xue and G. Zhu, Metal–organic framework membranes: from synthesis to separation application, *Chem. Soc. Rev.*, 2014, **43**(16), 6116–6140.
4 P. V. Alekseevskiy, A. Efimova, S. Povarov, N. A. Zhestkij, P. A. Demakov, N. Burzak, V. A. Dyachuk, V. P. Fedin, A. S. Potapov, X. Yu and V. A. Milichko, ., Fiber-Integrated Metal–Organic Framework Nanosheets for Light Emission and Microendoscopy, *ACS Appl. Nano Mater.*, 2026, **9**(4), 1860–1868.
5 H. Furukawa, K. E. Cordova, M. O'Keeffe and O. M. Yaghi, The Chemistry and Applications of Metal-Organic Frameworks, *Science*, 2013, **341**(6149), 1230444.
6 G. Chakraborty, I.-H. Park, R. Medishetty and J. J. Vittal, Two-Dimensional Metal-Organic Framework Materials: Synthesis, Structures, Properties and Applications, *Chem. Rev.*, 2021, **121**(7), 3751–3891.
7 P. V. Alekseevskiy, X. Yu, A. S. Efimova, N. A. Zhestkij, Y. A. Mezenov, Y. A. Kenzhebayeva, S. A. Povarov, A. Lubimova, S. V. Bachinin, E. A. Stepanidenko, V. Dyachuk, N. Li, V. P. Fedin, A. S. Potapov and V. A. Milichko, Ultrathin Lanthanide-Based Metal-Organic Nanosheets with Thickness- and Temperature-Driven Light Emission, *Laser Photonics Rev.*, 2025, **19**(12), 2401912.
8 Y. A. Mezenov, S. V. Bachinin, Y. A. Kenzhebayeva, A. S. Efimova, P. V. Alekseevskiy, D. Poloneeva, A. Lubimova, S. A. Povarov, V. Shirobokov, M. S. Dunaevskiy, A. S. Falchevskaya, A. S. Potapov, A. Novikov, A. A. Selyutin, P. Boulet, A. N. Kulakova and V. A. Milichko, Transformation of 3D Metal–Organic Frameworks into Nanosheets with Enhanced Memristive Behavior for Electronic Data Processing, *Adv. Sci.*, 2025, **12**(16), 2405989.
9 G. Swain, S. Sultana and K. Parida, A review on vertical and lateral heterostructures of semiconducting 2D-MoS2 with other 2D materials: a feasible perspective for energy conversion, *Nanoscale*, 2021, **13**(22), 9908–9944.
10 J. C. Tan and A. K. Cheetham, Mechanical properties of hybrid inorganic–organic framework materials: establishing fundamental structure–property relationships, *Chem. Soc. Rev.*, 2011, **40**(2), 1059–1080.
11 N. C. Burtch, J. Heinen, T. D. Bennett, D. Dubbeldam and M. D. Allendorf, Mechanical properties in metal–organic frameworks: emerging opportunities and challenges for device functionality and technological applications, *Adv. Mater.*, 2018, **30**(37), 1704124.
12 L. R. Redfern and O. K. Farha, Mechanical properties of metal–organic frameworks, *Chem. Sci.*, 2019, **10**(46), 10666–10679.
13 R. Dziobek-Garrett and T. J. Kempa, Excitons at the interface of 2D TMDs and molecular semiconductors, *J. Chem. Phys.*, 2024, **160**(20), 200902.
14 S. M. J. Rogge, S. Borgmans and V. Van Speybroeck, Absorbing stress via molecular crumple zones: Strain engineering flexibility into the rigid UiO-66 material, *Matter*, 2023, **6**(5), 1435–1462.
15 Q. Tu, I. Spanopoulos, E. S. Vasileiadou, X. Li, M. G. Kanatzidis, G. S. Shekhawat and V. P. Dravid, Exploring the Factors Affecting the Mechanical Properties of 2D Hybrid Organic–Inorganic Perovskites, *ACS Appl. Mater. Interfaces*, 2020, **12**(18), 20440–20447.
16 A. Jouneghaninaseri, S. Zhang, Q. Tu and J. Liu, Molecular engineering in layered metal halide hybrid perovskites for tunable thermal conductivity, elastic modulus, and beyond, *MRS Commun.*, 2025, **15**(6), 1307–1322.
17 W. C. Oliver and G. M. Pharr, An improved technique for determining hardness and elastic modulus using load and displacement sensing indentation experiments, *J. Mater. Res.*, 1992, **7**(6), 1564–1583.
18 J.-C. Tan, P. J. Saines, E. G. Bithell and A. K. Cheetham, Hybrid Nanosheets of an Inorganic–Organic Framework Material: Facile Synthesis, Structure, and Elastic Properties, *ACS Nano*, 2012, **6**(1), 615–621.
19 Y. Iwai, S. Kusumoto, R. Suzuki, M. Tachibana, K. Komatsu, T. Kikuchi, S. I. Kawaguchi, H. Kadobayashi, Y. Masubuchi, Y. Yamamoto, Y. Ozawa, M. Abe, K. Hirai, B. Le Ouay, M. Ohba and R. Ohtani, Mechanical Properties of Modulative Undulating Layers in Two-Dimensional Metal–Organic Frameworks, *Chem. Mater.*, 2024, **36**(11), 5446–5455.
20 L.-J. Ji, Y. Qin, D. Gui, W. Li, Y. Li, X. Li and P. Lu, Quantifying the Exfoliation Ease Level of 2D Materials via Mechanical Anisotropy, *Chem. Mater.*, 2018, **30**(24), 8732–8738.
21 H. Yuan, K. Li, D. Shi, H. Yang, X. Yu, W. Fan, P. J. S. Buenconsejo and D. Zhao, Large-Area Fabrication of Ultrathin Metal-Organic Framework Membranes, *Adv. Mater.*, 2023, **35**(18), 2211859.
22 C. Hermosa, B. R. Horrocks, J. I. Martínez, F. Liscio, J. Gómez-Herrero and F. Zamora, Mechanical and optical properties of ultralarge flakes of a metal–organic framework with molecular thickness, *Chem. Sci.*, 2015, **6**(4), 2553–2558.
23 H. Sahabudeen, Q. Zhang, Y. Liu, M. Heuchel and R. Machatschek, Mechanistic insights into the deformation and degradation of a 2D metal organic framework, *npj 2D Mater. Appl.*, 2023, **7**(1), 25.
24 J. Lu, Y. Yoshida, K. Kanamori and H. Kitagawa, Robust Proton Conduction against Mechanical Stress in Flexible Free-Standing Membrane Composed of Two-Dimensional Coordination Polymer, *Angew. Chem., Int. Ed.*, 2023, **62**(34), e202306942.
25 Z. Zheng, C. S. Ruiz-Vargas, T. Bauer, A. Rossi, P. Payamyar, A. Schütz, A. Stemmer, J. Sakamoto and A. D. Schlüter, Square-Micrometer-Sized, Free-Standing Organometallic Sheets and Their Square-Centimeter-Sized Multilayers on Solid Substrates, *Macromol. Rapid Commun.*, 2013, **34**(21), 1670–1680.

26 H. Sahabudeen, H. Qi, B. A. Glatz, D. Tranca, R. Dong, Y. Hou, T. Zhang, C. Kuttner, T. Lehnert, G. Seifert, U. Kaiser, A. Fery, Z. Zheng and X. Feng, Wafer-sized multifunctional polyimine-based two-dimensional conjugated polymers with high mechanical stiffness, *Nat. Commun.*, 2016, **7**(1), 13461.

27 V. F. Yusuf, N. I. Malek and S. K. Kailasa, Review on metal–organic framework classification, synthetic approaches, and influencing factors: applications in energy, drug delivery, and wastewater treatment, *ACS Omega*, 2022, **7**(49), 44507–44531.

28 H. Ghasempour, K.-Y. Wang, J. A. Powell, F. ZareKarizi, X.-L. Lv, A. Morsali and H.-C. Zhou, Metal–organic frameworks based on multicarboxylate linkers, *Coord. Chem. Rev.*, 2021, **426**, 213542.

29 H. Li, M. Eddaoudi, M. O'Keeffe and O. M. Yaghi, Design and synthesis of an exceptionally stable and highly porous metal-organic framework, *Nature*, 1999, **402**(6759), 276–279.

30 J. H. Cavka, S. Jakobsen, U. Olsbye, N. Guillou, C. Lamberti, S. Bordiga and K. P. Lillerud, A new zirconium inorganic building brick forming metal organic frameworks with exceptional stability, *J. Am. Chem. Soc.*, 2008, **130**(42), 13850–13851.

31 C. Lee, X. Wei, J. W. Kysar and J. Hone, Measurement of the Elastic Properties and Intrinsic Strength of Monolayer Graphene, *Science*, 2008, **321**(5887), 385–388.

32 A. Falin, Q. Cai, E. J. Santos, D. Scullion, D. Qian, R. Zhang, Z. Yang, S. Huang, K. Watanabe and T. Taniguchi, Mechanical properties of atomically thin boron nitride and the role of interlayer interactions, *Nat. Commun.*, 2017, **8**(1), 15815.

33 S. Bertolazzi, J. Brivio and A. Kis, Stretching and Breaking of Ultrathin MoS2, *ACS Nano*, 2011, **5**(12), 9703–9709.

34 D. Kim, E. K. Qian, D. G. Chica, Y.-H. Chiang, M. G. Kanatzidis and Q. Tu, Mechanical Properties of 2D LiInP2Se6: Implication for Semiconductor Applications, *ACS Appl. Nano Mater.*, 2023, **6**(10), 8214–8221.

35 Q. Tu, I. Spanopoulos, P. Yasaei, C. C. Stoumpos, M. G. Kanatzidis, G. S. Shekhawat and V. P. Dravid, Stretching and Breaking of Ultrathin 2D Hybrid Organic–Inorganic Perovskites, *ACS Nano*, 2018, **12**(10), 10347–10354.

36 D. Kim, E. S. Vasileiadou, I. Spanopoulos, X. Wang, J. Yan, M. G. Kanatzidis and Q. Tu, Unveiling the Fatigue Behavior of 2D Hybrid Organic–Inorganic Perovskites: Insights for Long-Term Durability, *Adv. Sci.*, 2023, **10**(26), 2303133.

37 Q. Fang, Z. Pang, Q. Ai, Y. Liu, T. Zhai, D. Steinbach, G. Gao, Y. Zhu, T. Li and J. Lou, Superior mechanical properties of multilayer covalent-organic frameworks enabled by rationally tuning molecular interlayer interactions, *Proc. Natl. Acad. Sci. U. S. A.*, 2023, **120**(15), e2208676120.

38 M. Bagherzadeh, F. Ashouri and M. Đaković, Synthesis, structural characterization and application of a 2D coordination polymer of Mn-terephthalate as a heterogeneous catalyst for olefin oxidation, *Polyhedron*, 2014, **69**, 167–173.

39 D. Kim, E. S. Vasileiadou, I. Spanopoulos, M. G. Kanatzidis and Q. Tu, Abnormal In-Plane Thermomechanical Behavior of Two-Dimensional Hybrid Organic–Inorganic Perovskites, *ACS Appl. Mater. Interfaces*, 2023, **15**(6), 7919–7927.

40 A. S. Efimova, P. V. Alekseevskiy, M. V. Timofeeva, Y. A. Kenzhebayeva, A. O. Kuleshova, I. G. Koryakina, D. I. Pavlov, T. S. Sukhikh, A. S. Potapov, S. A. Shipilovskikh, N. Li and V. A. Milichko, Exfoliation of 2D Metal-Organic Frameworks: toward Advanced Scalable Materials for Optical Sensing, *Small Methods*, 2023, **7**(11), 2300752.

41 D. A. Walters, J. P. Cleveland, N. H. Thomson, P. K. Hansma, M. A. Wendman, G. Gurley and V. Elings, Short cantilevers for atomic force microscopy, *Rev. Sci. Instrum.*, 1996, **67**(10), 3583–3590.

42 J. L. Hutter and J. Bechhoefer, Calibration of atomic–force microscope tips, *Rev. Sci. Instrum.*, 1993, **64**(7), 1868–1873.

43 M. Edgar, R. Mitchell, A. M. Z. Slawin, P. Lightfoot and P. A. Wright, Solid-State Transformations of Zinc 1,4-Benzenedicarboxylates Mediated by Hydrogen-Bond-Forming Molecules, *Chem. – Eur. J.*, 2001, **7**(23), 5168–5175.

44 Z. Jiang, Y. An, X. Zhu, C. Tian, J. Bai and Y. Li, Solvent-Dependent Synthesis from Layer to Microporous Pillared-Layer Framework for Selective Sorption of Gas Light Hydrocarbons, *Z. Anorg. Allg. Chem.*, 2015, **641**(15), 2599–2603.

45 S. R. Batten, N. R. Champness, X.-M. Chen, J. Garcia-Martinez, S. Kitagawa, L. Öhrström, M. O'Keeffe, M. P. Suh and J. Reedijk, Terminology of metal–organic frameworks and coordination polymers (IUPAC Recommendations 2013), *Pure Appl. Chem.*, 2013, **85**(8), 1715–1724.

46 D. Kim, E. S. Vasileiadou, I. Spanopoulos, M. G. Kanatzidis and Q. Tu, In-plane mechanical properties of two-dimensional hybrid organic–inorganic perovskite nanosheets: structure–property relationships, *ACS Appl. Mater. Interfaces*, 2021, **13**(27), 31642–31649.

47 A. Castellanos-Gomez, M. Poot, G. A. Steele, H. S. J. Van Der Zant, N. Agraït and G. Rubio-Bollinger, Elastic properties of freely suspended MoS2 nanosheets, *Adv. Mater.*, 2012, **24**, 772–775.

48 U. Komaragiri, M. Begley and J. Simmonds, The mechanical response of freestanding circular elastic films under point and pressure loads, *J. Appl. Mech.*, 2005, **72**(2), 203–212.

49 Q. Tu, D. Kim, M. Shyikh and M. G. Kanatzidis, Mechanics-coupled stability of metal-halide perovskites, *Matter*, 2021, **4**(9), 2765–2809.

50 P. Canepa, K. Tan, Y. Du, H. Lu, Y. J. Chabal and T. Thonhauser, Structural, elastic, thermal, and electronic responses of small-molecule-loaded metal–organic framework materials, *J. Mater. Chem. A*, 2015, **3**(3), 986–995.

51 Q. Wei and X. Peng, Superior mechanical flexibility of phosphorene and few-layer black phosphorus, *Appl. Phys. Lett.*, 2014, **104**(25), 251915.

52 R. Yang, L. Mei, Z. Lin, Y. Fan, J. Lim, J. Guo, Y. Liu, H. S. Shin, D. Voiry, Q. Lu, J. Li and Z. Zeng, Intercalation

in 2D materials and in situ studies, *Nat. Rev. Chem.*, 2024, **8**(6), 410–432.

53 R. Namakian, M. A. Garzon, Q. Tu, A. Erdemir and W. Gao, Temperature-Induced Phase Transition in 2D Alkylammonium Lead Halide Perovskites: A Molecular Dynamics Study, *ACS Nano*, 2024, **18**(34), 22926–22937.

54 Q. Tu, I. Spanopoulos, S. Hao, C. Wolverton, M. G. Kanatzidis, G. S. Shekhawat and V. P. Dravid, Out-of-plane mechanical properties of 2D hybrid organic–inorganic perovskites by nanoindentation, *ACS Appl. Mater. Interfaces*, 2018, **10**(26), 22167–22173.

55 Q. Hao, C. Zhao, B. Sun, C. Lu, J. Liu, M. Liu, L.-J. Wan and D. Wang, Confined synthesis of two-dimensional covalent organic framework thin films within superspreading water layer, *J. Am. Chem. Soc.*, 2018, **140**(38), 12152–12158.

56 Q. Fang, C. Sui, C. Wang, T. Zhai, J. Zhang, J. Liang, H. Guo, E. Sandoz-Rosado and J. Lou, Strong and flaw-insensitive two-dimensional covalent organic frameworks, *Matter*, 2021, **4**(3), 1017–1028.

57 M. F. Ashby, *Materials Selection in Mechanical Design 4th ed*, Elsevier, 2011.

58 (*a*) CCDC 2522895: Experimental Crystal Structure Determination, 2026, DOI: 10.5517/ccdc.csd.cc2qp8qf; (*b*) CCDC 2522896: Experimental Crystal Structure Determination, 2026, DOI: 10.5517/ccdc.csd.cc2qp8rg.